Chapter 4

Visible to near-infrared spectroscopy and device characterisation

Previous measurements performed on the wings of butterflies with microstructured wing scales were limited by the techniques used, which for specific angles of incidence either showed the spectral reflectivity [16, 17, 19, 20, 21], the angular distribution of the scattered field at one wavelength [17] or a large-aperture spectral measurement of portions of the backscattered light [18], thus failing to provide a complete and consistent optical characterisation of the studied structures. The results produced only a partial picture of the phenomenology associated with the scales of their specimen and led to incomplete modelling and interpretation of the physics behind it.

In this chapter, a technique will be presented, which enables low-aperture measurements of the near-complete scattered field of a sample at any wavelength, polarisation and angle of incidence. This setup involved the employment of photonic crystal fibres and the construction of a high-precision and flexible alignment rig. After a qualitative analysis of the optical properties of the tropical butterfly *Morpho rhetenor*, a quantitative characterisation will follow of both the natural specimen and artificial samples.

4.1 Qualitative analysis

A first glance of the wings of *Morpho rhetenor* reveals immediately a feature which has struck both zoologists and physicists for over a century: the color is a remarkably intense 'metallic' blue, no matter what the position of the viewer is.

To illustrate this quality, photographs of a portion of the wing of this butterfly are shown in figure 4.1. The six photographs were taken under different conditions of lighting and collection with a digital camera Minolta Dimage 7i, and successively a set of statistical data were extrapolated from high-luminosity areas of the photographs using a photographic computer processing package (Jasc Paint Shop Pro Version 6.02). These were average values over the lightness domain (0 to 255) of the histograms for the luminance and the red, green and blue pixel counts. The apertures of both

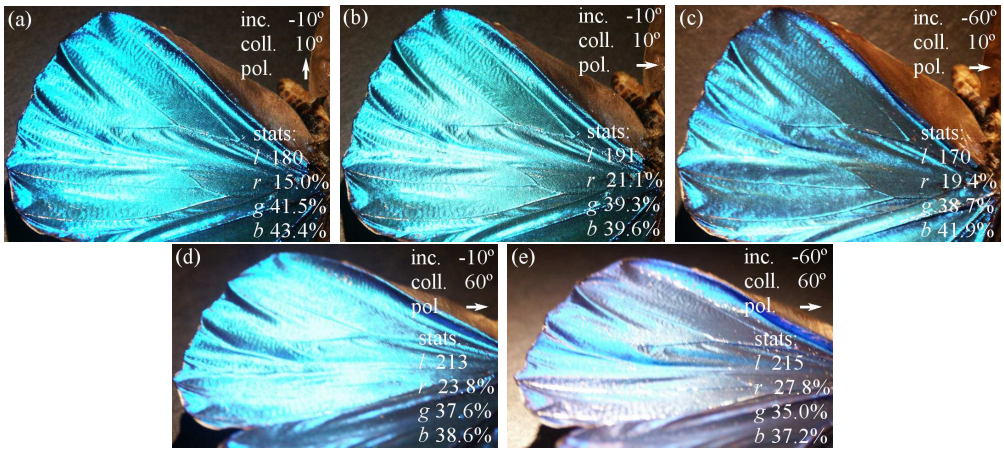

Figure 4.1: Photographs of a portion of the wing of *Morpho rhetenor* taken under different conditions of lighting and collection. The wing was lit with unpolarised, white light incident at $-10°$ (a, b and d) and $-60°$ (c and e) with respect to the wing normal. The pictures were taken at an angle of collection of $10°$ (a to c) and $60°$ (d and e) with respect to the wing normal, and with a linear polariser filter oriented vertically (a) and horizontally (b to e). The statistical data reported are average values of the luminance (l), red (r), green (g) and blue (b) content of pixels extrapolated from the histogram of each digital picture (photos by Luca Plattner).

the light source and the camera objective are rather large and thus the indicated angles are only approximative average values, nonetheless this allows us to control some viewing parameters whilst maintaining the nature of a visual inspection. Also, the ridges of the microstructure on the wing scales are very similarly oriented over large domains, but the collective orientation can vary from domain to domain across the wing, thus preventing a relation between the directions of incidence and collection, and the orientation of the microstructure from being established.

Comparison of the photographs (a) and (b) of figure 4.1, both taken at an angle of incidence of $-10°$, shows how changing the orientation of a linear polariser filter (Hoya PL) mounted on the camera objective when the wing is lit with white, unpolarised light causes a distinct if not dramatic change in the hue of the acquired picture. This chromatic effect equally occurs at other angles of incidence and shows that the appearance of the wing is related to the polarisation of light. The photographs (b) and (c) are taken with the filter oriented horizontally and show the effects of changing the angle of incidence of the light, passing from a specular view to a non-specular one, for which the angles of incidence and collection differ. The overall appearance changes, but wide areas of the wing still shine a 'metallic' blue, with modest variations of both the luminance and the proportions of primary colours from one case to the other. A similar situation is found for a large angle of viewing ($60°$) as shown in the photographs (d) and (e) also taken with the filter oriented horizontally. In this case, the luminance is highly increased with respect to a small angle of incidence not only for the expected case of specular reflection (e), but also for non-specular collection (d), and the wing is more homogenously brilliant for the latter. In both cases, luminance and hue are comparable for the high luminosity areas, with the exception of an increase of the red colour in the specular case. Similar behaviour is observed for the filter oriented vertically.

In conclusion, from a qualitative analysis, in which the subjectivity of the observer's judgement and the spectral response of the instrument used

cannot be neglected, it was established that light with similar intensities is scattered by the wing microstructure over large solid angles covering most of the incidence hemisphere irrespective of the angle of incidence. A certain degree of polarisation was found in the specularly reflected light at small angles of incidence.

4.2 Experimental setup

To overcome the limitations of previous experimental investigations of the optical properties of diffractive samples, a novel setup was built, which involved the use of a fibre source of coherent white light and the construction of a goniometer capable of positioning samples with high accuracy.

The design of this system achieved the following seven main targets:

- Characterisation of sample scattering in the plane of incidence over a near full 360° range of angles.
- Use of coherent white light for the source illumination.
- Micron scale beam-focussing/sampling capability.
- Five degrees of freedom sample positioning with nanometer scale accuracy.
- Control and flexibility of incident beam direction, position and polarisation.
- Control and flexibility of direction, position, aperture and polarisation of the collected scattered field.
- Absolute power density measurements through accurate referencing and gauging.

4.2.1 Near full 360° light scattering spectroscopy

The main difficulty in building a goniometer to measure the scattering of light from sample areas only few microns in size lies in the need to maintain the alignment of the optics with microscopic accuracy when changing the angle between the normal to the sample surface and the optical path of collection with a macroscopic rig.

With the usual construction of a goniometer consisting of a ring fitted to a shaft, the tolerances of the precision machining equipment exceed an accuracy of centering for the two objects of $\pm 30 \mu m$ using a running fit. Such accuracy is unacceptable when the optical paths along two arms of the goniometer must meet at its center in a space of only a few microns. For this reason, a system of conically shaped shafts and rings was designed that made the machining tolerances irrelevant to the centering problem. The principle is that a conic ring placed on a conic shaft having the same slope self-centers and the manufacturing tolerances result in an uncertainty in the relative position of the two parts along their rotation axes (*i.e.* in their heights) and not normally to them. By choosing appropriate materials, high-quality steel for the shaft and hardened, high-quality aluminium for the ring, a mechanically stable system was built, which exhibited a centering accuracy beyond the sensitivity of any mechanical measurement device available. In consideration of the load applied to the ring in the setup, which amounted to a few kilograms, an optimal slope of 10° was chosen for the cones, thus providing a mechanism that with appropriate lubrication does not lock and runs smoothly.

Based on this principle, a goniometer was designed and machined that could be mounted on an optical table and support optical components with a metric fitting system. The design is presented in appendix D and photographs showing the assembled setup are given in figure 4.2. The rig had three concentric conical rings mounted on a unique shaft with a stepped conical profile, the rings being vertically shifted with respect to each other and the top one included a platform to mount optical components. An arm was

fixed to each ring, thus resulting in two independent rotating beams and one solidly connected to the rotating platform (the incidence arm), all bound to the same axis of rotation and extending $550mm$ from it. The arms were provided with standard threaded holes to fit optical components and adjustable supporting legs at their end to precisely regulate the flatness and guarantee the stability of the ring mechanism. Finally, all aluminium parts were hard anodised.

A system of linear and rotary stages allowed control with nanometer scale precision of the position and orientation of the samples with 5 degrees of freedom. This was important to ensure that the micrometer-sized area of the sample to be investigated was placed exactly on the centre of rotation of the rig, where the optical paths of the incident beam and the collection cone meet. Also, the angle of incidence (*Euler* angle ϕ) was determined via one rotary stage, since the platform was solidly fixed to the arm supporting the optics of the incidence beam, and the orientation of the sample surface with respect to the the plane of incidence (*Euler* angle θ) was adjustable via a second rotary mechanism.

For the purpose of spectroscopic measurements, a photonic crystal fibre (PCF) was employed to provide a mobile source of coherent white light using a previously unreported technique. In a similar way to the examples discussed in section 1.7.2, the PCF was pumped with a high-power, ultrashort infrared (IR) pulsed signal obtained by a regenerative titanium sapphire (Ti:Sa) amplified laser source. This produced an $800nm$ wavelength seed for the supercontinuum (SC) generation in the PCF, having a pulse width of $FWHM = 150fs$, a repetition frequency of $250kHz$ and a time-averaged power of $10mW$. This corresponds to a peak power of $26.7kW$ and an energy per pulse of $4nJ$. The IR beam was coupled into the PCF using a $60\times$ microscope objective and a high-accuracy xyz positioning stage. The output end of the PCF was mounted on the incidence arm of the rig and was capable of following every movement without restraint or loss of power. Photographs and a schematic of the experimental setup are shown in figures 4.2 and 4.3.

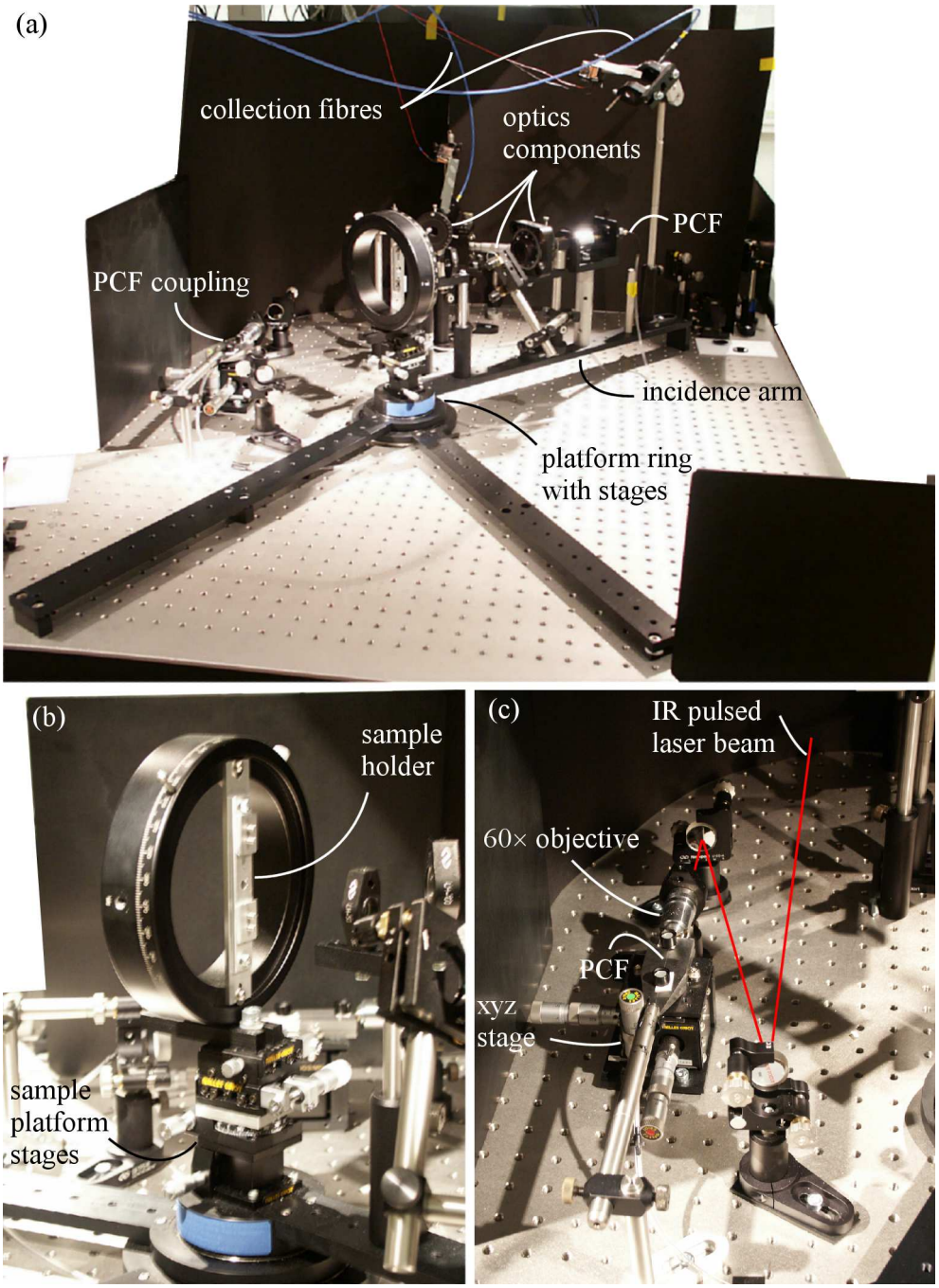

Figure 4.2: Photographs of the experimental rig. Overview (a), detail of the sample holder and the sample positioning stages mounted on the platform ring (b), and detail of the PCF coupling arrangement (c).

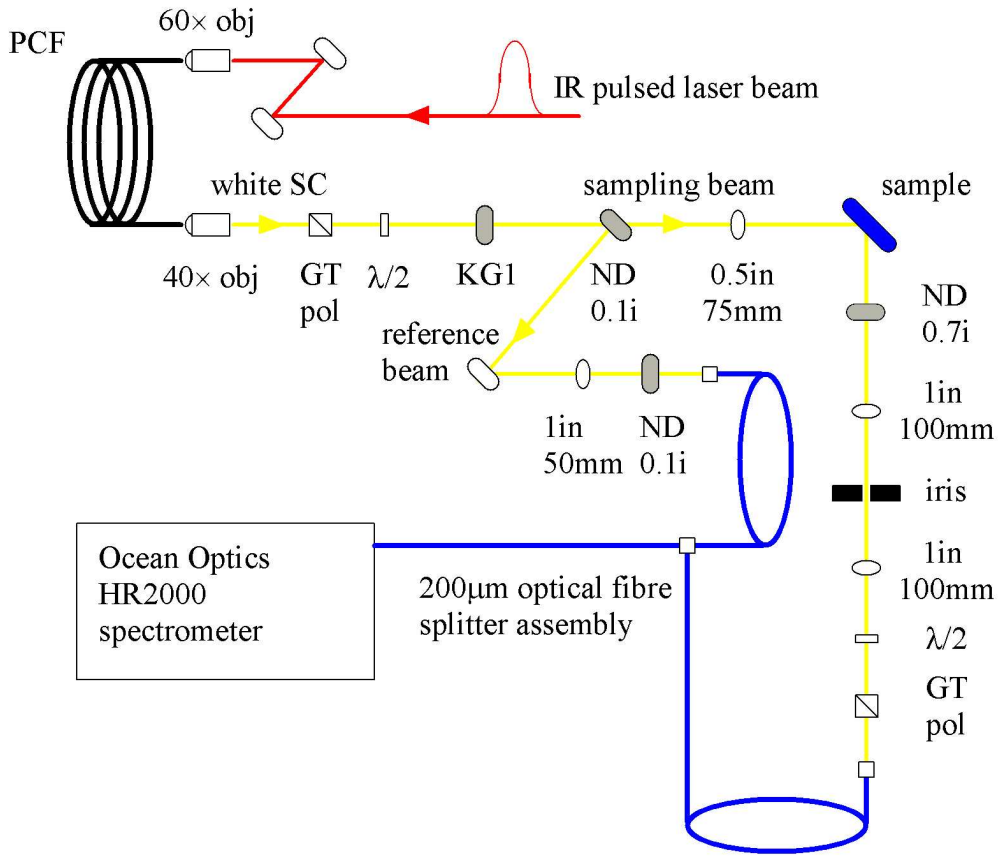

Figure 4.3: Schematic diagram of the experimental setup.

The white SC escaping the PCF's output was collimated using a 40× objective and the moderate polarisation of the beam was made complete with a *Glan-Taylor* polariser (GT). The linear polarisation of the beam was then controlled via a $\lambda/2$ plate and the IR spectral content reduced with a high-pass filter (KG1). About 10% of its power was then removed for referencing purposes with an achromatic filter (inconel-NiCrFe ND 0.1) and once focussed, it was collected by one branch of a bifurcated optical fibre attached to the incidence arm and feeding into the spectrometer. The incident beam was focussed onto the sample by a $0.5in$ achromatic lens with a focal length of $75mm$.

The field scattered by the sample in the plane of incidence was collected over a solid angle determined by an iris mounted on the optical table and the direction of collection was varied by changing the position of the incidence arm. The aperture of the collected beam was $0.64srad$. The beam was collimated, its polarisation controlled with a further polariser and a $\lambda/2$ plate, attenuated if necessary to a suitable power, and finally focussed onto the second branch of the optical fibre feeding into the same spectrometer. All the optics involved were achromatic to exploit optimally the white light source. The remaining achromaticity of the setup was gauged via the reflectance of a high-quality achromatic mirror and all measurements were scaled accordingly. The high-resolution spectrometer was an Ocean Optics HR2000, with a $10\mu m$ slit, a $300l/mm$ grating and a resolution of $1nm$, and was connected to via a splitter assembly of $200\mu m$ core, single strand optical fibres. The light scattered from the surface of a sample could be measured over nearly 360°, with the exception of a blind spot, an arc extending $\pm 10°$ from the direction of the incident beam which was due to a limitation in movement of the incidence arm caused by the collection optics.

A measurement of the reference beam was performed immediately before each acquisition of scattering data in order to minimise the effects of fluctuations in the spectral content of the incident beam and obtain accurate relative measurements. Each acquired spectrum was also corrected for intrinsic achromaticity of the set up, gauged through reflection measurements of a high-quality mirror. The low-aperture ($6 \cdot 10^{-4} srad$) incident beam was focussed to a beam-waist ($FWHM$) of $(30 \pm 5)\mu m$.

4.2.2 A fibre source of coherent white light

A $2m$-long piece of PCF with a nominal core diameter of $2\mu m$ and a total diameter without cladding of $125\mu m$ was pumped with a high-power, IR pulsed seed (described in section 4.2.1) to generate an SC optimised for visible applications, stretching from 400 to $900nm$. A cross-section SEM view of this fibre is shown in figure 1.12 of chapter 1 and a typical spectrum

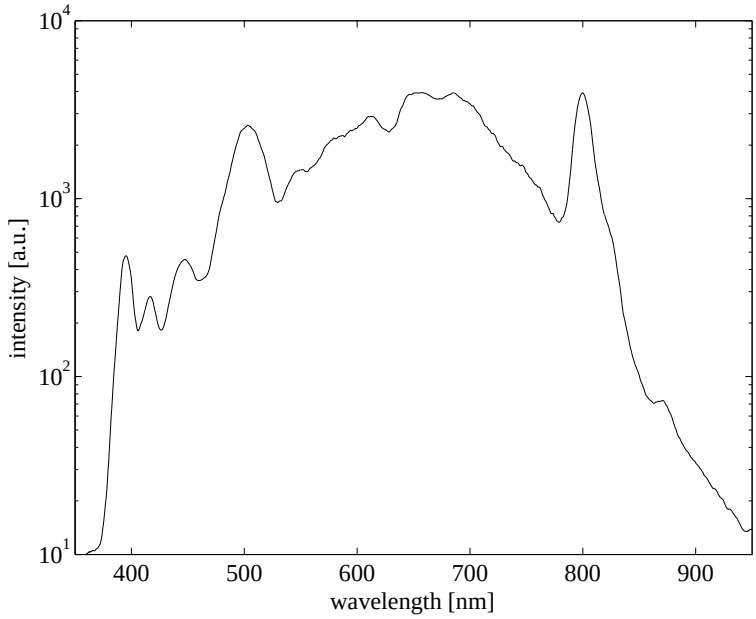

Figure 4.4: Spectrum of SC obtain from a PCF and used for spectroscopy purposes.

is shown in figure 4.4.

This source provided an excellent white light SC, comparable in quality to the results of published work [83, 86, 87] discussed in section 1.7.2, which was ideally suited to the measurement setup, supplying a reliable and flexible mobile source for experiments which require a prolonged operation.

4.3 Light scattering of *Morpho* wing

With the setup discussed in section 4.2, measurements of the light scattering from the wings of *Morpho rhetenor* when incident at various angles and with different polarisations were performed. A small portion of a wing was attached to a flat surface and fixed in the sample holder. The ridges of the microstructure were oriented parallel to the axis of rotation of the rig, such as to be normally oriented with respect to the plane of incidence. This was achieved by projecting the scattered field onto a cylindrical screen, which resulted in a horizontal line, as expected from a grating-like structure, when

the wing was inclined at an approximate angle of 20° due to the slanting of the layering discussed in section 1.2.2 [19]. In this way it was also possible to ensure that the focussed incident beam was contained completely within the area of a single scale, since overlapping two scales invariably resulted in a split diffraction pattern. Performing the measurements at angles of scattering between the grazing angle on one side of the wing normal to the grazing angle on the other side ensured that the surface of the microstructure was oriented within an accuracy of ±5° from the expected direction. Measurements were performed for angles of incidence of 10°, 30° and 60°. The polarisation of the incident and scattered beams was either parallel (TM) or perpendicular (TE) to the plane of incidence. No noticeable effects of cross-polarisation of the scattered field were detected at any of the investigated angles of incidence, therefore in future only measurements will be discussed where the polarisations of incidence and collection are equal.

The samples were characterised measuring the scattering at directions 5° apart and covering all the directions in the plane of incidence between −85° and 85° with exception of the blind spot of the measurement setup. Since the solid angle of collection corresponded to a cone with a slope of about 2.5°, the scattering was sampled with a high angular resolution without any gaps left other than the blind spot. Figure 4.6 shows filled contour plots for all the measurements with the angle of scattering and the light wavelength as coordinates, where the color-coded intensity of the two-dimensional scattering spectrogram is scaled to the reflection of a high-quality achromatic mirror representing the value 1 and the intensity is plotted on a logarithmic scale. The grey areas correspond to the blind spot of the setup.

The majority of the scattered power is found at wavelengths shorter than $550nm$, with the longer wavelengths being highly transmitted by the microstructure. For different polarisations similar distributions of power are found in the spectrograms, with locally different patterns and higher values for the TM polarisation. In general, most of the scattered power is found at angles close to the incident one and the wing microstructure acts as a

retro-reflector irrespective of the orientation of its surface. At an incident angle of 10°, two lobes are found in the angular distribution of the scattered power, one located around 40° and one approximately around −20°, the second more intense than the first. At the higher angles of incidence, the lobe in the positive range of angles disappeared, the overall intensity of the stronger features decreased with increasing angle of incidence and the lobe in the negative range of angles is split in two. Also, at all angles of incidence the angular spreading is increased with decreasing wavelengths and for the TE polarisation a background band of constant intensity extends over most of the measured range of angles for wavelengths around $430nm$, where part of the split lobe is centered. For an angle of incidence of 60°, more light is back-scattered at longer wavelengths, again forming a band extending over a wide angular range.

The modest values of the intensity of the scattered light are due to the small aperture of the measurements, whereby a change in the aperture of the scattered field has dramatic effects on the amount of collected power. Hence, while all of the incident power is collected by the scattered beam, and measured when using the mirror, for a diffractive structure the power is distributed over a wider range of angles of scattering. The butterfly wing scatters the incident power continuously over 180°, which results in lower power densities per unit angle. Figure 4.5 shows the total reflection of the butterfly wing microstructure for angles of incidence of 10°, 30° and 60°, and both polarisations. These plots corresponds to integrating the spectrograms in figure 4.6 over the whole range of angles, with the exception of the angles in the blind spot.

The results obtained for an angle of incidence of 10° agree with published results [17] obtained under similar conditions (normal incidence). Both studies show similar relative spectral contents of the total reflection and similar angular distributions of the scattering. The reported values for the total reflection, obtained with an integrating sphere and at normal incidence, were higher than those given in figure 4.5, which correspond to an integration over

only a portion of the hemisphere of incidence, not accounting for scattering out of the plane of incidence and for the blind spot.

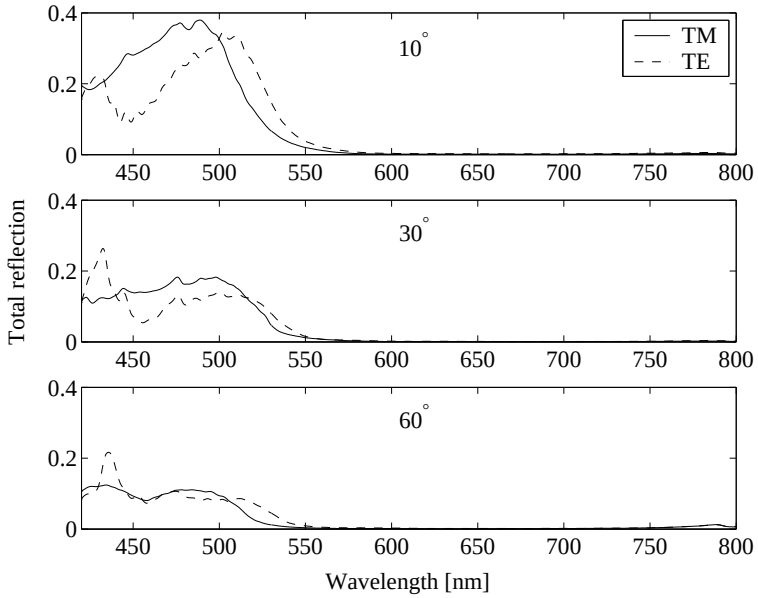

Figure 4.5: Total reflection of *Morpho rhetenor* microstructure for angles of incidence of 10°, 30° and 60°, and both polarisations.

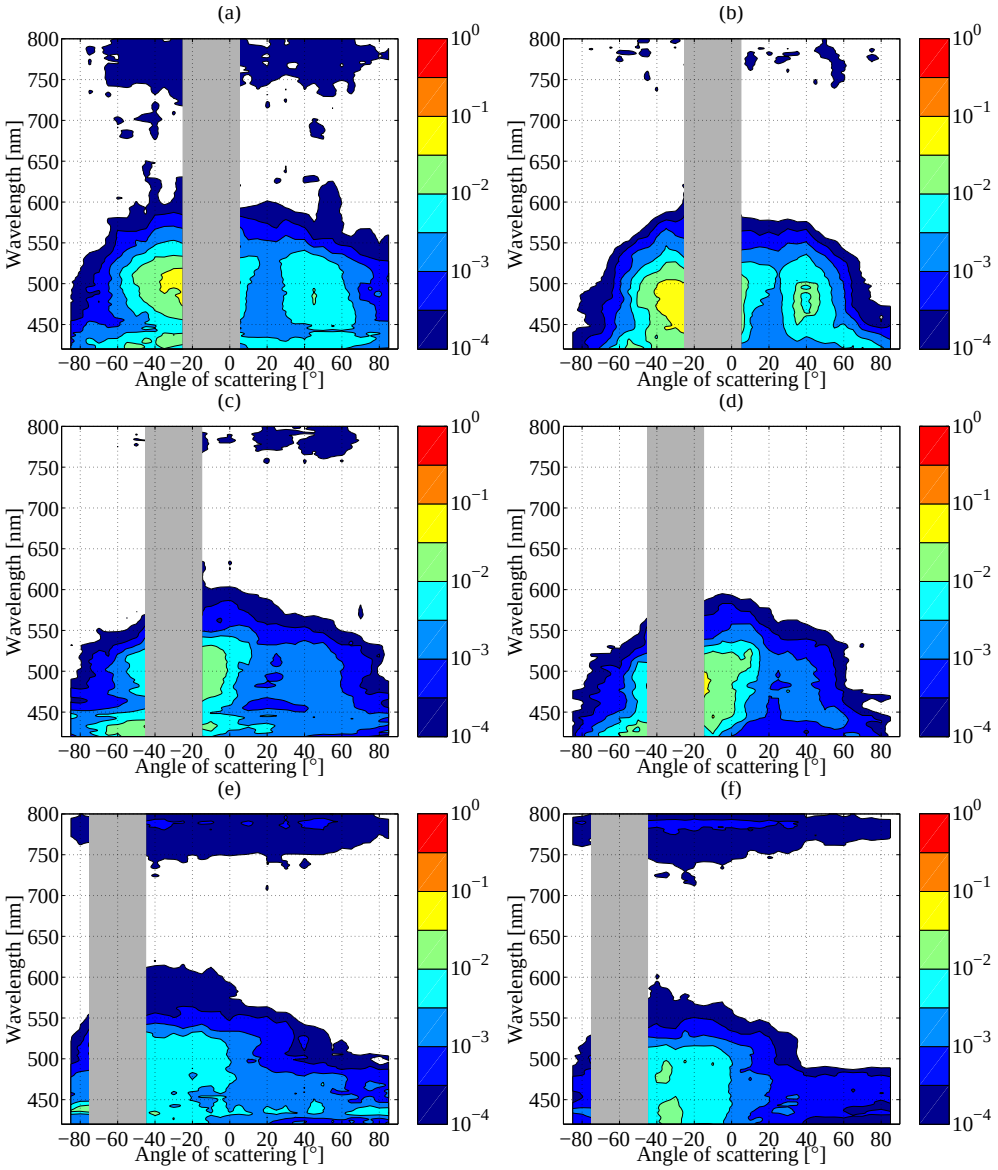

Figure 4.6: Filled contour plots of the scattering off the surface of the wings of *Morpho rhetenor* at different angles of incidence and polarisation. (a) and (b) 10° incidence, (c) and (d) 30° incidence, (e) and (f) 60° incidence. (a), (c) and (e) TE polarisation, (b), (d) and (f) TM polarisation. The grey areas correspond to the blind spot of the measurement setup.

4.4 Light scattering of two-dimensional surface photonic crystals

One of the fabricated volume diffractive structures, a $510nm$-period lamellar grating with layered diffractive elements as discussed in section 3.3, was also characterised using the same method employed for the butterfly microstructure. The sample was attached flatly to the sample holder and the ridges of the grating-like structure were oriented parallel to the axis of rotation of the rig, such as to be normally oriented with respect to the plane of incidence. Measurements were performed for angles of incidence of 10°, 30° and 60°. The polarisation of the incident and scattered beams was either parallel (TM) or perpendicular (TE) to the plane of incidence. No noticeable effects of cross-polarisation of the scattered field were detected at any of the investigated angles of incidence. Figure 4.7 shows filled contour plots for all the measurements representing spectrograms comparable to those discussed in section 4.3. The values are again scaled to the reflectivity of a high-quality mirror and the gray area corresponds to the blind spot of the setup.

Two features are immediately apparent when viewing the spectrograms: a medium-intensity background spreads over large angular and spectral ranges, particularly for the TE polarisation; and the diffraction orders appear very modulated. The bands of high angular spread are visible by the naked eye when projecting the scattered field on a cylindrical screen and appear as a white line extending continuously over most of the range of angles in the plane of incidence. This feature is qualitatively similar to the scattering of light off a single, sharp edge of dielectric material and can consequently be attributed to the presence in the diffractive structures of many sharp edges, namely the boundaries between dielectric and air. The modulation of the diffraction orders can be further studied by looking at their spectra, shown in figure 4.8. The spectrum of the 0^{th} order or reflectance does not exhibit the high-reflectivity band found in the non etched dielectric mirrors particularly at the lower angles of incidence. This is best illustrated comparing

the reflectance of the diffractive structure for light incident 30° (plot (b) of figure 4.8) with that of the dielectric mirror characterised under the same conditions of incidence shown in left-hand side of figure 3.3. Due to the modest dielectric filling fraction of the device (20%), the filtering action of the vertical modulation is reduced. Much of the incident light is transmitted through to the substrate and reflected back by silicon. However, due to the lateral distribution, a large portion of the backscattered power is found in the first order of diffraction, which is strongly modulated. The intensity distribution in the spectra is also strongly dependent on the polarisation, a property which results in polarisation extinction ratios of up to 340.

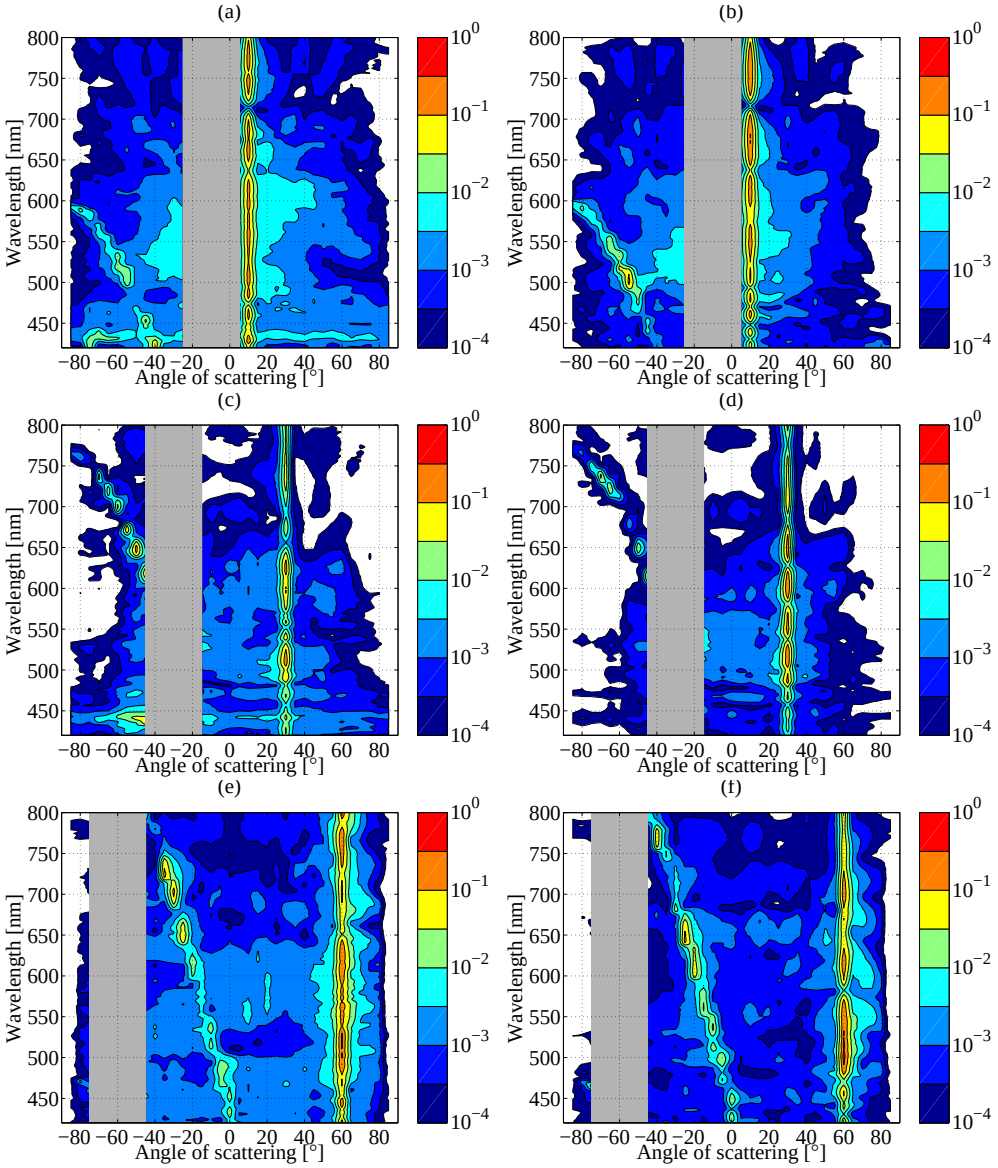

Figure 4.7: Filled contour plots of the scattering off the surface of a fabricated volume diffractive structure with a grating pitch of $510nm$ at different angles of incidence and polarisation. (a) and (b) 10° incidence, (c) and (d) 30° incidence, (e) and (f) 60° incidence. (a), (c) and (e) TE polarisation, (b), (d) and (f) TM polarisation. The grey areas correspond to the blind spot of the measurement setup.

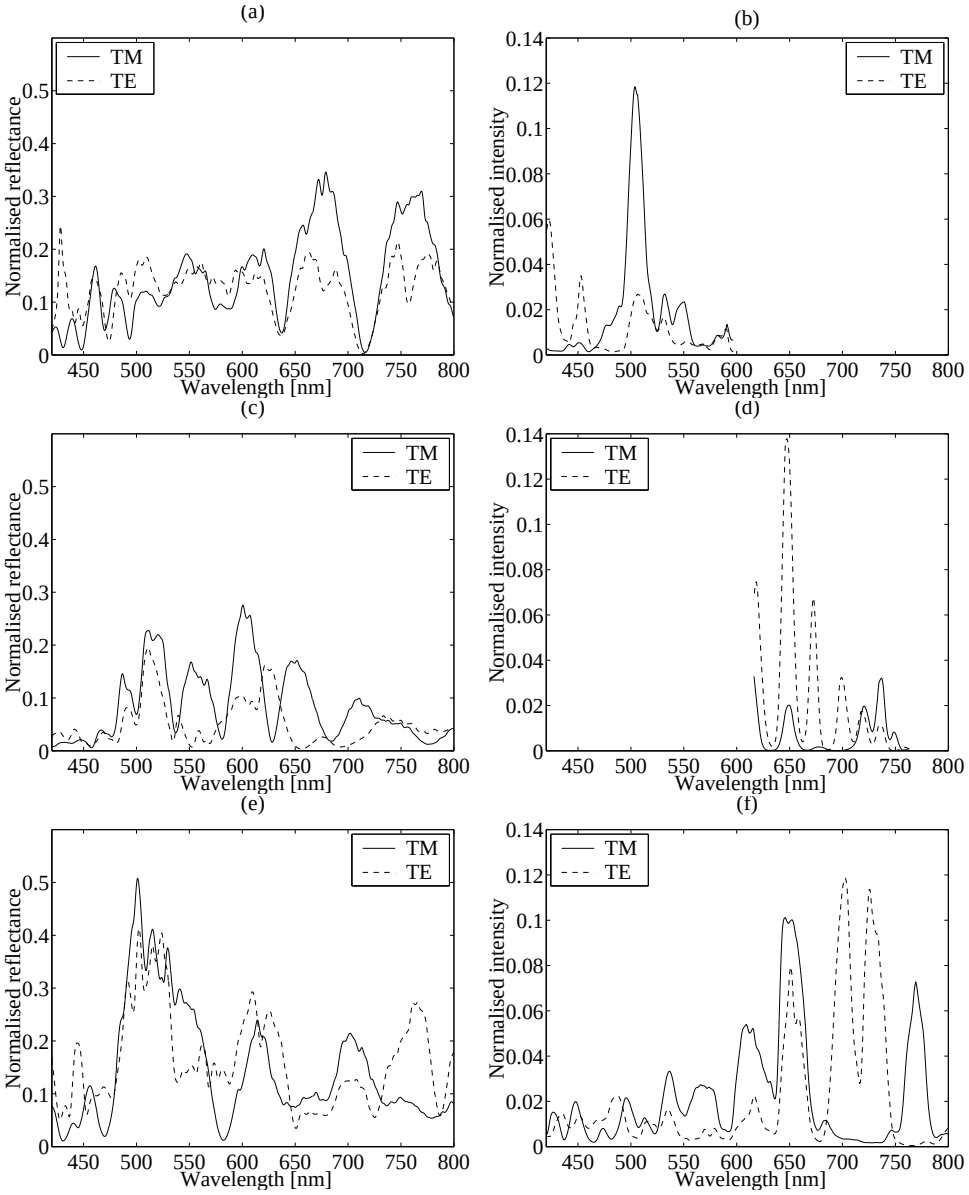

Figure 4.8: Spectra of reflective 0^{th} and 1^{st} diffraction orders for all investigated conditions of incidence. Plots (a), (c) and (e) show the 0^{th} diffraction order, or specular reflection, for an angle of incidence of $10°$, $30°$ and $60°$, respectively. Plots (b), (d) and (f) show the corresponding 1^{st} diffraction orders. All values are normalised to the reflectance of a high-quality mirror.

4.5 Conclusion

A novel measurement technique has been developed, which allows one to characterize the scattering from a sample surface on the near complete circle of directions in the plane of incidence, at all angles of incidence, polarisations and wavelengths, in the visible and near-infrared part of the spectrum. To achieve this an originally designed goniometer was built, which enables micron scale alignment of the optical axes of the incident beam, the scattering collection optics and the sample surface, and a mobile source of coherent white light was implemented in the experimental setup using a PCF.

The optical properties of the wing of the tropical butterfly *Morpho rhetenor* have been qualitatively analysed by visual inspection and quantitatively characterised by means of the above mentioned measurement technique. A fabricated sample has been equally characterised under the same conditions and with the same methodology used for the butterfly.

The interpretation of the butterfly phenomenology and its impact on the understanding of the mechanisms of colour production will be discussed in chapter 6.